The effects of proliferation status and cell cycle phase on the responses of single cells to chemotherapy

Adrián E. Granada[a,b,*], Alba Jiménez[b], Jacob Stewart-Ornstein[b,c], Nils Blüthgen[a,d,e,f], Simone Reber[a,g], Ashwini Jambhekar[b], and Galit Lahav[b]

[a]IRI Life Sciences, Humboldt University Berlin, 10115 Berlin, Germany; [b]Department of Systems Biology, Harvard Medical School, Boston, MA 02115; [c]Department of Computational and Systems Biology, University of Pittsburgh Medical School, Pittsburgh, PA 15260; [d]Institute of Pathology, Charité Universitätsmedizin Berlin, 10117 Berlin, Germany; [e]German Cancer Consortium (DKTK), German Cancer Research Center (DKFZ), 69120 Heidelberg, Germany; [f]Berlin Institute of Health (BIH), 10178 Berlin, Germany; [g]University of Applied Sciences Berlin, 13353 Berlin, Germany

ABSTRACT **DNA-damaging chemotherapeutics are widely used in cancer treatments, but for solid tumors they often leave a residual tumor-cell population. Here we investigated how cellular states might affect the response of individual cells in a clonal population to cisplatin, a DNA-damaging chemotherapeutic agent. Using a live-cell reporter of cell cycle phase and long-term imaging, we monitored single-cell proliferation before, at the time of, and after treatment. We found that in response to cisplatin, cells either arrested or died, and the ratio of these outcomes depended on the dose. While we found that the cell cycle phase at the time of cisplatin addition was not predictive of outcome, the proliferative history of the cell was: highly proliferative cells were more likely to arrest than to die, whereas slowly proliferating cells showed a higher probability of death. Information theory analysis revealed that the dose of cisplatin had the greatest influence on the cells' decisions to arrest or die, and that the proliferation status interacted with the cisplatin dose to further guide this decision. These results show an unexpected effect of proliferation status in regulating responses to cisplatin and suggest that slowly proliferating cells within tumors may be acutely vulnerable to chemotherapy.**

Monitoring Editor
Rong Li
Johns Hopkins University and National University of Singapore

Received: Sep 16, 2019
Revised: Jan 31, 2020
Accepted: Feb 6, 2020

INTRODUCTION

Cells within a single tumor or tissue display great diversity at their epigenetic, transcriptomic, and proteomic states. Even in genetically homogeneous cells, these internal factors alone can generate significant phenotypic and behavioral heterogeneity, leading to variation in response to drug stimuli (Albeck *et al.*, 2008; Spencer *et al.*, 2009; Sharma *et al.*, 2010). Tumor cells exposed to chemotherapeutic DNA-damaging agents show a wide range of responses: at the intermediate EC50 dose, for example, cells show maximally divergent outcomes, with half surviving and half succumbing. The cellular features that promote one cell fate outcome or the other include internal cellular states (Inde and Dixon, 2018) and the stochastic nature of DNA damage (Hanahan and Weinberg, 2011; Fumagalli *et al.*, 2012). In addition, different DNA-damaging agents generate sets of specific types of DNA legions (e.g., single- or double-strand breaks, cross-links) in various genomic locations, which in turn affect a cell's ability to recover (Noll *et al.*, 2006; Fumagalli *et al.*, 2012). Recent studies of sister cells suggest that the strongest contributor to the diversity of responses to DNA damage is the internal state of the cell: its protein, RNA, and epigenomic states (Chakrabarti *et al.*, 2018). Individual cell fate choices therefore are shaped by the distribution of cellular states across the tumor and collectively determine the overall response to therapy.

This article was published online ahead of print in MBoC in Press (http://www.molbiolcell.org/cgi/doi/10.1091/mbc.E19-09-0515) on February 12, 2020.

Author contributions: A.E.G., J.S.O., N.B., S.R., and G.L. conceived and designed the experiments; A.E.G. performed the experiments; A.E.G. and Alba Jiménez analyzed the data; A.E.G., J.S.O., Ashwini Jambhekar, and G.L. drafted the article; A.E.G. and Alba Jiménez prepared the digital images.

*Address correspondence to: Adrián E. Granada (adrian.granada@charite.de).

Abbreviations used: CFP, cyan fluorescent protein; IMT, intermitotic time; NLS, nuclear localization signal; Prol, proliferation; SSPI, single-cell proliferation index; YFP, yellow fluorescent protein.

Traditional assays of cellular response to chemotherapy involve analyzing the expression of proliferation markers in fixed cells, and therefore cannot link the proliferation outcomes to the prior states of the cells. Live microscopy that follows the response of individual cells to treatment over time has identified preexisting cell-state features (e.g., expression of MYC or cell cycle phase) that impact cellular outcomes in mammalian systems (Paek *et al.*, 2016; Ryl *et al.*, 2017; Chatzopoulou *et al.*, 2018). Studies tracking multiple cell generations and sister cells over time as they respond to DNA damage and drug compounds suggest that multigeneration long-term memory features dominate cellular outcome choices (Arora *et al.*, 2017; Chakrabarti *et al.*, 2018; Korsnes and Korsnes, 2018; Wolff *et al.*, 2018). These studies show a relation between cell state and the fate of cells after stimulus, but the specific variables explored in each study (e.g., p53 signaling or circadian rhythm) only explain a minor (though significant) portion of the observed variation, suggesting that our understanding of the contribution of the internal cell state to cell fate is still missing important features.

Two major sources of diversity across genotypically similar cancer cells in vitro and in vivo are cell cycle phase and overall proliferative rate (Driessens *et al.*, 2012; Yano *et al.*, 2014). These two factors have long since been linked to sensitivity to general chemotherapy (Hill and Baserga, 1975; Hoshino *et al.*, 1975). Cell cycle phase-specific cytotoxic drugs differentially target cells based on proliferative status (Amadori *et al.*, 1997; Baguley *et al.*, 1995). This observation is rationalized in terms of selective killing: highly proliferative cancer cells pass through their sensitive cell cycle phases more frequently during the treatment time window, thereby increasing their likelihood of being damaged by the cytotoxic agent (Berenbaum, 1972). Recent studies using cell cycle phase-specific drugs have contradicted this view, but no alternative models have yet succeeded in solving this paradox (Noguchi, 2006; Mitchison, 2012). Despite the long-recognized importance of the cycle phase and proliferative rate for treatment response, there have been few efforts to disentangle their contributions, and it remains unknown how they interact to impact the specific outcome.

Cisplatin, one of the most effective and broadly used chemotherapeutic drugs, damages DNA by inducing both inter- and intrastrand cross-links, as well as protein–DNA cross-links. Cisplatin is a cross-linker chemotherapeutic agent and its cytotoxic effects are conventionally considered to be agnostic of the cell cycle (Rupniak *et al.*, 1983; Zamble and Lippard, 1995). Despite its success, many tumors still react poorly and/or develop resistance to cisplatin (Galluzzi *et al.*, 2012). At a cellular level, cisplatin generates heterogeneous responses with cells either dying or arresting. This heterogeneous outcome has been proposed to lead to cancer cell persistence (Luong *et al.*, 2016; Shen *et al.*, 2013). Moreover, the duration and dose of cisplatin treatment affect both the overall degree of cytotoxicity and the cell cycle phase at which the resistant cells arrest (He *et al.*, 2011; Rupniak *et al.*, 1983). The effects of internal cellular states on regulating the balance between cell cycle arrest or death in response to cisplatin treatment remain poorly understood.

Here, we studied how cell cycle phase and proliferation status contribute to determining cellular outcomes of human cells in response to cisplatin. We tracked the proliferation behavior and cell cycle progression in hundreds of asynchronously growing cells and dissected the effects of cell cycle phase and proliferation status at the time of treatment. Using information theory analysis, we found that cell cycle phase had minimal influence on cellular outcomes. Proliferation status showed synergistic interactions with cisplatin dose in shaping the balance of cellular outcomes. Our work has thus dissected the contributions of different aspects of cellular physiology in guiding cellular outcomes in response to cisplatin.

RESULTS

Cisplatin induces heterogeneous dose-dependent cell fate choices

The standard approaches to studying drug responses mainly use bulk population measurements and single-time snapshots to estimate proliferation status. Recent work has highlighted the limitations of such population- and time-averaged indirect measures of responses to chemotherapeutic drugs (Tyson *et al.*, 2012; Hafner *et al.*, 2016). To address these limitations, we used live long-term high–temporal resolution assays and tracked human bone osteosarcoma epithelial cells (U2OS) 2 d before and 5 d after drug addition (Figure 1A). Different cisplatin doses resulted in a monotonic dose-dependent reduction in proliferation with varied kinetics of the response (Figure 1, B and C). Specifically, low to intermediate doses (Figure 1C, b–f) resulted in delayed exponential-like growth whereas high doses (Figure 1C, g–l) induced a smooth drop followed by a plateau in cell numbers. In addition, low to intermediate doses led to a graded decrease in proliferation, whereas higher doses clustered together, showing less than a fivefold increase in cell number at concentrations above 2 μM (g to l), a signature of a nonlinear dose response (see details of the response curve in Supplemental Figure S1). These proliferation dynamics can result from multiple underlying time-dependent effects, including asynchronously triggered heterogeneous cell fate choices with different intrinsic time scales. Indeed, the DNA-damaging agent cisplatin is known to halt proliferation by inducing both cell death and cell cycle arrest (Siddik, 2003; Galluzzi *et al.*, 2012; Paek *et al.*, 2016; Martins *et al.*, 2018). To determine the contribution of cell death and cell cycle arrest to the observed proliferation curves, we turned to higher-resolution live-cell microscopy.

We first sought to quantify the cisplatin dose–dependent distributions of cell fate choices. We conducted a series of short-term, high-resolution microscopy experiments and monitored cell fate outcomes over time at three different cisplatin doses (0, 7, 10, and 13 μM, referred to as control, low, medium, and high doses, respectively). We implemented a Kaplan–Meier survival analysis using death and division as events, and right-censoring for cells that did not die nor divide within the 3 d (see *Materials and Methods*). The fraction of dying cells increased over time at all doses, with the extent of cell death being dose-dependent (Figure 1D). Notably, a lag of approximately 24 h occurred at all concentrations before cell death was observed, possibly reflecting the time required for induction and execution of cell death programs. The fraction of dividing cells showed a more abrupt dose-dependent decrease, with even the lowest dose of cisplatin reducing cell division below 50% of the control (Figure 1E).

Our long-term live-cell imaging allowed us to analyze the specific cellular trajectories preceding arrest or death (Figure 1F). Specifically, we found that untreated cells typically proliferated throughout the observation period, undergoing multiple cell divisions, with only a small fraction (8.4%) dying (Figure 1G). Cisplatin-treated cells died or arrested either after undergoing a single division or without executing any cell divisions. The proportion of cells dividing more than once after cisplatin treatment was negligible (less than 1%). We therefore classified cells into six cellular phenotypes (Figure 1F) according to whether they proliferated, arrested, or died and the number of cell divisions occurring before the terminal outcome. Note that cisplatin-treated cells did not undergo

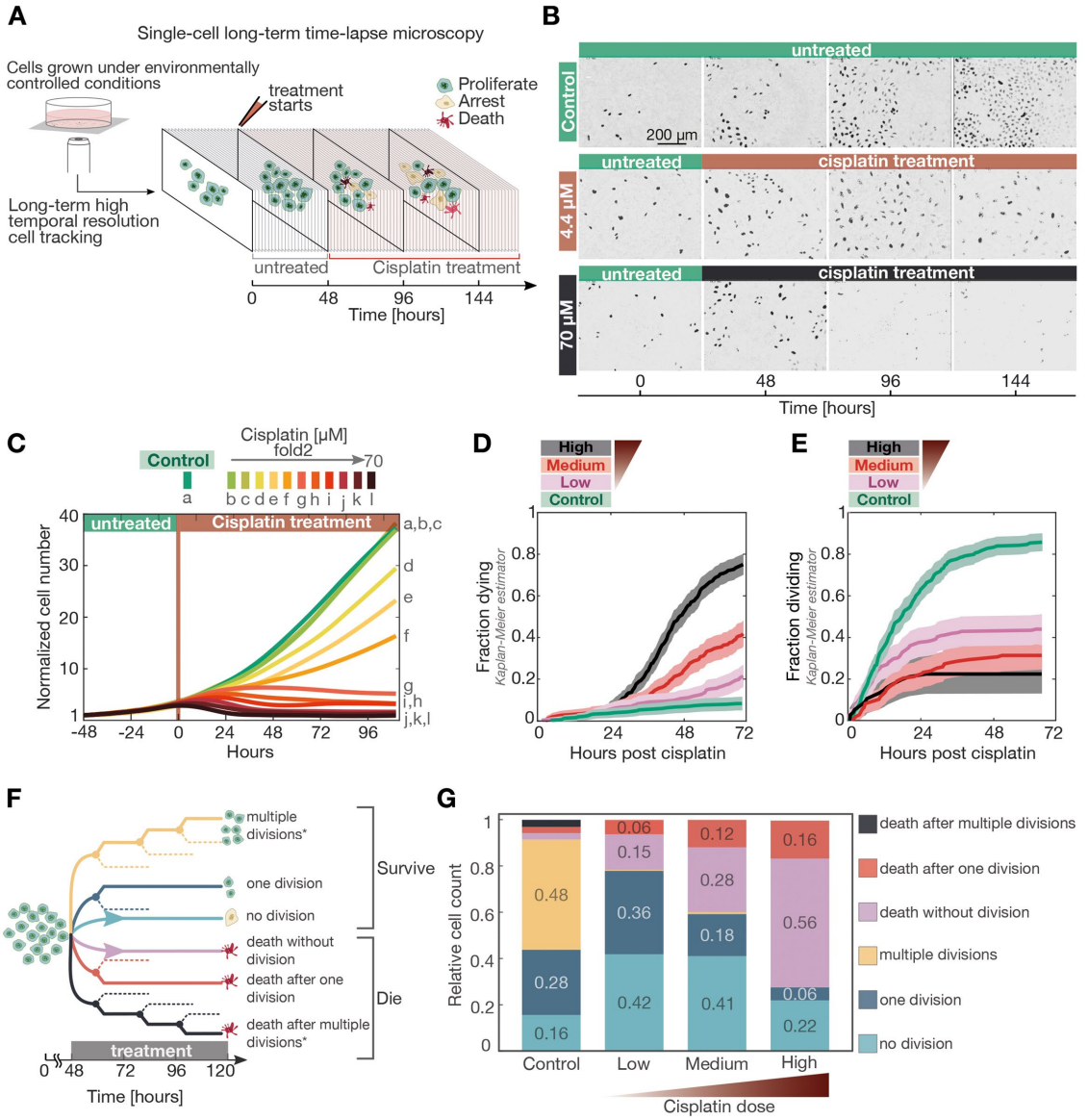

FIGURE 1: Cisplatin induces dose-dependent heterogeneous cell fate outcomes. (A) Schematic of the experimental setup. Cells were continuously monitored using a fluorescence microscope for up to 7 d under environmentally controlled conditions. After 2 d, cells were treated with cisplatin and their outcomes were monitored. (B) Sample images of control or cisplatin-treated cells taken every 48 h. Cells were untreated or treated with 4.4 or 70 μM cisplatin. (C) Normalized cell number over time in cultures treated with a gradient of cisplatin doses. Colored lines represent the response to each cisplatin dose (untreated control "a" in dark green, lowest dose "b" in light green, and highest dose "l" in black). Doses range from 70 to 0.07 μM in twofold decrements (70, 35, 17.5 μM, etc.). Each growth curve was normalized to the number of cells at $t = -48$ h. Cell tracking started at $t = -48$ h with $n = 280–320$ cells tracked at 30-min intervals for a total of 7 d. Data were pooled from two replicates per dose. (D) Fraction of dying cells using the Kaplan–Meier estimator method for control, low, medium, and high cisplatin doses of 0, 7, 10, and 13 μM cisplatin, respectively. Shaded area along curves represents 95% confidence intervals. Cisplatin was added at $t = 0$ and individual cells were tracked for the following 3 d at 30-min intervals. (E) Fraction of dividing cells calculated using the Kaplan–Meier estimator method for those cells that undergo one or more mitosis events after cisplatin treatment, monitored as described in D. (F) Cellular outcomes were annotated and classified into six categories. For cells that divided, one of the two daughter cells was randomly selected for further tracking. Asterisk denotes outcomes that were only observed in the untreated cells. (G) Frequency of each outcome for each cisplatin dose. Final fractions were computed relative to the cell number before treatment (N_0). $n = 300$ (control), 262 (low-dose), 247 (medium-dose), and 316 (high-dose) individual cells.

multiple divisions and therefore exhibited only four of these phenotypic outcomes (Figure 1F). We computed the distribution of each cellular outcome for increasing cisplatin doses. As expected, higher cisplatin doses increased the dying fraction (Figure 1G). The fraction of arrested cells showed a nonmonotonic response: it increased compared with control cell and then decreased with increasing cisplatin dose, with the highest dose reaching a value even below that of the control population (Figure 1G). These experiments revealed the complex role of treatment strength in shifting the population balance between various cellular outcomes.

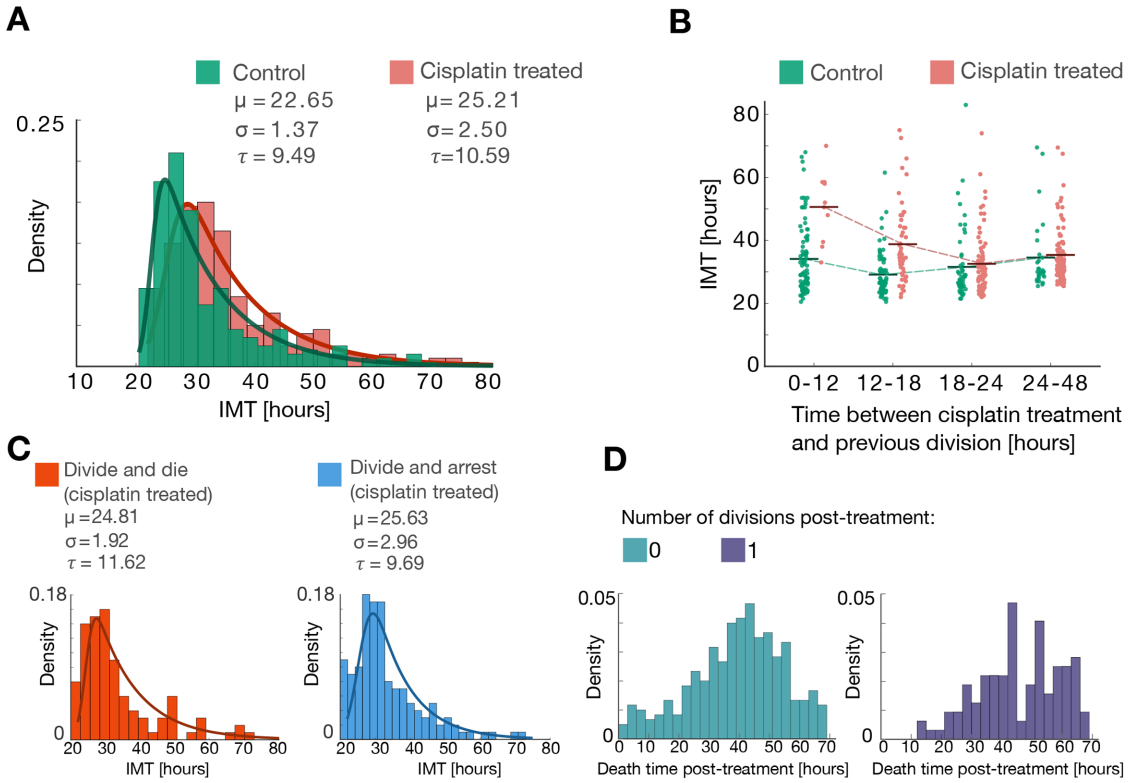

FIGURE 2: Cisplatin treatment at early stages of the cell cycle delays cell division. (A) Representative IMT distributions of untreated versus treated populations, measured from the first mitosis before cisplatin addition to the first mitosis after treatment (or mock treatment). Distributions were fitted to an EMG model. Legend: μ, mean of the Gaussian component of EMG; σ, deviation of the Gaussian component of EMG; τ, mean of the exponential component of EMG. A total of 242 IMTs were analyzed in each condition. To compare EMG distributions we used the Mann–Whitney U test, a nonparametric test of the null hypothesis that does not require the assumption of normal distributions. The *p* value of the two-sample Mann–Whitney U-test ($p < 0.05$, $p = 1.43 \times 10^{-7}$) indicates statistical significance in the differences in IMT between damaged and control cells. (B) IMT as a function of time between cisplatin treatment and previous division. (C) IMT distribution of treated cells that either arrest or die after division. The *p* value of the two-sample Mann–Whitney U-test ($p > 0.05$, $p = 0.9614$) indicates no statistical significance in the differences in IMT between cells that "divide and arrest" and those that "divide and die." (D) Time of death after treatment in cells that do (1 division) or do not divide (0 divisions) after treatment.

Cell divisions do not affect the timing or choice of final cellular outcomes

We first investigated the effects of cisplatin on cell division. Cisplatin suppressed cell division, as nearly 80% of treated cells failed to divide after treatment at the highest dose, whereas only 16% of untreated cells did not divide in the equivalent time period (Figure 1G). To determine the effect of cisplatin on cell cycle progression, we measured the intermitotic time (IMT) between the last division before cisplatin addition and the first division after. To adequately capture the variability in IMT distributions, we chose an exponentially modified Gaussian (EMG; Luce, 1986) model, which has been used to fit IMT distributions from a wide range of cells and conditions (Tyson *et al.*, 2012). The data are approximated as a combination of a Gaussian function with an exponential function to account for skewing of the right-side tail. This model uses only three parameters that are mathematically and biologically separable, as evidenced by the fact that their values are differentially affected by various drugs (Tyson *et al.*, 2012). The first two parameters, μ and σ, correspond to the mean and SD of the Gaussian component and can be interpreted as localization and variability indicators. The third parameter, τ, is the mean of the exponential component and corresponds to the right "tail" of the distribution, where a large τ implies a more skewed distribution. This analysis of IMTs revealed that cisplatin treatment resulted in a slight delay in the time of division, with a significant difference of approximately 3 h in the mean deviation of the Gaussian component (Figure 2A). We further investigated whether the delay depended on how long after mitosis cisplatin treatment was initiated, reasoning that cells receiving cisplatin early in their cell cycle may respond differently than those receiving it later (Figure 2B). Indeed, we found that cisplatin treatment soon after mitosis, that is, at the start of the next cell cycle, largely prevented cell division (few cells divided when treated at 0–12 h after completing the first mitosis; those that divided did so with a delay of nearly 20 h; Figure 2B). In contrast, cisplatin addition at later stages had no effect, likely because cells had already committed to division (Figure 2B, 24–48 h category). When added 12 to 18 h after mitosis, cisplatin delayed cell division by 9.6 h (Figure 2B). These results reveal a generally suppressive effect of cisplatin on cell division, with a G2 population of cells that is insensitive to this effect.

Having established that cisplatin treatment negatively affected cell division, we next determined whether undergoing mitosis in the presence of cisplatin affected the final cellular outcomes of arrest or death. The distribution of these outcomes was not different between the populations of cells that did and did not undergo mitosis

	Death	Arrest	Ratio
High			
No mitosis	177	59	3.00
Mitosis	51	17	3.00
Medium			
No mitosis	74	100	0.74
Mitosis	32	48	0.66
Low			
No mitosis	32	105	0.31
Mitosis	20	85	0.26

TABLE 1: Death-to-arrest ratio dependence on mitosis for different cisplatin doses.

after cisplatin treatment (Table 1). Cells that arrested, as well as those that died, showed equivalent IMTs, indicating that IMT was not a predictor of final outcomes (Figure 2C). We next investigated whether undergoing division affected the time of cell death. We found that the distribution of death times was equivalent between the dividing and nondividing populations (Figure 2D). These results suggest that undergoing cell division does not influence the choice of final cellular outcomes or the timing of the decision. We have therefore continued our analysis classifying only two outcomes, arrest or death, regardless of the presence or absence of cell divisions preceding these outcomes.

Responses to cisplatin are independent of cell cycle phase

Having established that cell cycle phase at the time of cisplatin addition influenced whether cells would divide (Figure 2), we next investigated whether cell cycle phase also affects the final outcomes. To assess cell cycle phase, we created an isogenic U2OS cell line carrying an hGeminin-CFP fluorescent nuclear marker, which is absent during G1, increases at the onset of S, further accumulates through S and G2 and sharply degrades during mitosis (Sakaue-Sawano *et al.*, 2008; Figure 3A). We verified that in U2OS cells hGeminin-CFP was a faithful cell cycle marker and that our analysis of cellular Geminin trajectories could separate cells by cycle phase (Supplemental Figure S2A). We tracked cell cycle progression in individual asynchronously growing cells for 2 d. We then treated them with the three different doses of cisplatin as described above and annotated their cell fate outcomes during the 3 d following treatment (Figure 3B). Upon each cell division, one of the daughter cells was randomly selected for further tracking. We used the Geminin trajectories before treatment to cluster cells based on their cell cycle phase (G1, S, or G2) and further sorted each category into two cell fate outcomes: arrest or death. We calculated the arrest and death ratios and color-coded the bars by the treatment dose (Figure 3, C and D; Supplemental Tables 1–5). As expected, and observed earlier (Figure 1), cisplatin induced cell death in a dose-dependent manner (Figure 3C). However, this analysis revealed minor effects between cell cycle phase and the final outcome (Figure 3C) or the timing of cell death (Supplemental Figure S2B). The minor role of cell-cycle on final outcomes agrees with the classification of cisplatin as a cross-linker agent, generally considered to be cell cycle–nonspecific agents.

Single-cell proliferation index modulates cellular outcomes

In addition to cell cycle phases, cells also possess a less well-defined proliferative state, which has been proposed to contribute to their response to chemotherapeutics (Lin, 1973; Valeriote and Putten, 1975; Stover *et al.*, 2016). Proliferative states are often measured by immunohistochemistry of proliferation markers such as Ki76 or PCNA, and proliferation has since long been identified as a prognostic clinical marker (Tannock, 1978; Tubiana *et al.*, 1984). Our live-cell imaging of untreated cells revealed that cells exhibited substantial heterogeneity in their proliferative behavior, even in the absence of cisplatin treatment. Specifically, cells divided between 0 and 5 times over the 5 d of imaging (Supplemental Figure S3A), with cells dividing fewer times showing a larger rightward skew in their distribution of IMTs ($\tau = 10.97$ for cells dividing three times vs. 1.33 for cells dividing five times), while the mean component of the Gaussian distribution, μ, remained stable independent of the number of cell divisions (Supplemental Figure S3A). To address whether proliferation status at the time of cisplatin treatment affected the cellular response, we classified cells into nondividers (0 divisions), low-proliferative (1 division), and high-proliferative (>2 divisions) categories, based on their trajectories within the first 48 h of imaging before cisplatin addition. We named this metric the single-cell proliferation index (SSPI; Figure 4A), in analogy to the tumor proliferation index. To determine the stability of the SSPI, we determined it over the course of 2 d and compared it with the SSPI that was determined during the course of the next 2 d in untreated cells. This analysis revealed that while the nondividing state was stable (no nondividers divided in the subsequent 2 d; Figure 4B, S3B), some cells in the high- and low-SSPI categories switched states (Figure 4B). Low-proliferation cells were equally likely to switch into each of the three proliferation categories, but high-proliferation cells were most likely to remain proliferative and showed a low frequency of switching into the nondividing class. This trend was also reflected in the median number of divisions by each group over time (Supplemental Figure S3B). The timescales of cellular states in the absence of perturbation resemble the timescales observed in the levels of individual proteins. In human cells, protein expression levels fluctuated over the course of less than one to over two generations (Sigal *et al.*, 2006). Such variations in protein levels, particularly in those regulating the cell cycle, may underlie the observed switching between proliferation states.

We next investigated whether proliferation state influenced cell fate outcomes in response to cisplatin (Figure 4, C–E, and Supplemental Tables 6–8). We excluded the nondividing (ND) category, as it contained a negligible fraction of cells (approximately 10 cells, representing <2% of the population; see Supplemental Table 6). The landscape of outcomes showed a more complex topology than that observed across cell cycle phases. High cisplatin doses led primarily to cell death for both high- and low-proliferation categories. However, at low and medium cisplatin doses, the two proliferation categories showed differences in their distribution of outcomes. High-proliferation cells were less likely to die than low-proliferation cells (death ratios of 0.43 vs. 0.17 at low dose, and 0.58 vs. 0.35 at medium dose, for low- and high-proliferation cells, respectively; Figure 4D), thus tipping the outcome of high-proliferation cells toward arrest (Figure 4E). These results show that at low doses, low-proliferation cells are 2.5 times more likely to die than high-proliferation cells (Figure 4D). Note that even though low-proliferation cells were more likely than high-proliferation cells both to die and to arrest when untreated (Figure 4, D and E), cisplatin addition altered these trends and elevated the arrest ratio of high-proliferation cells above that of low-proliferation cells (Figure 4E). We next investigated whether proliferation status affected the time of cell death and found that high-proliferation cells died slightly later than low-proliferation cells (Supplemental Figure S3C). Together, our results

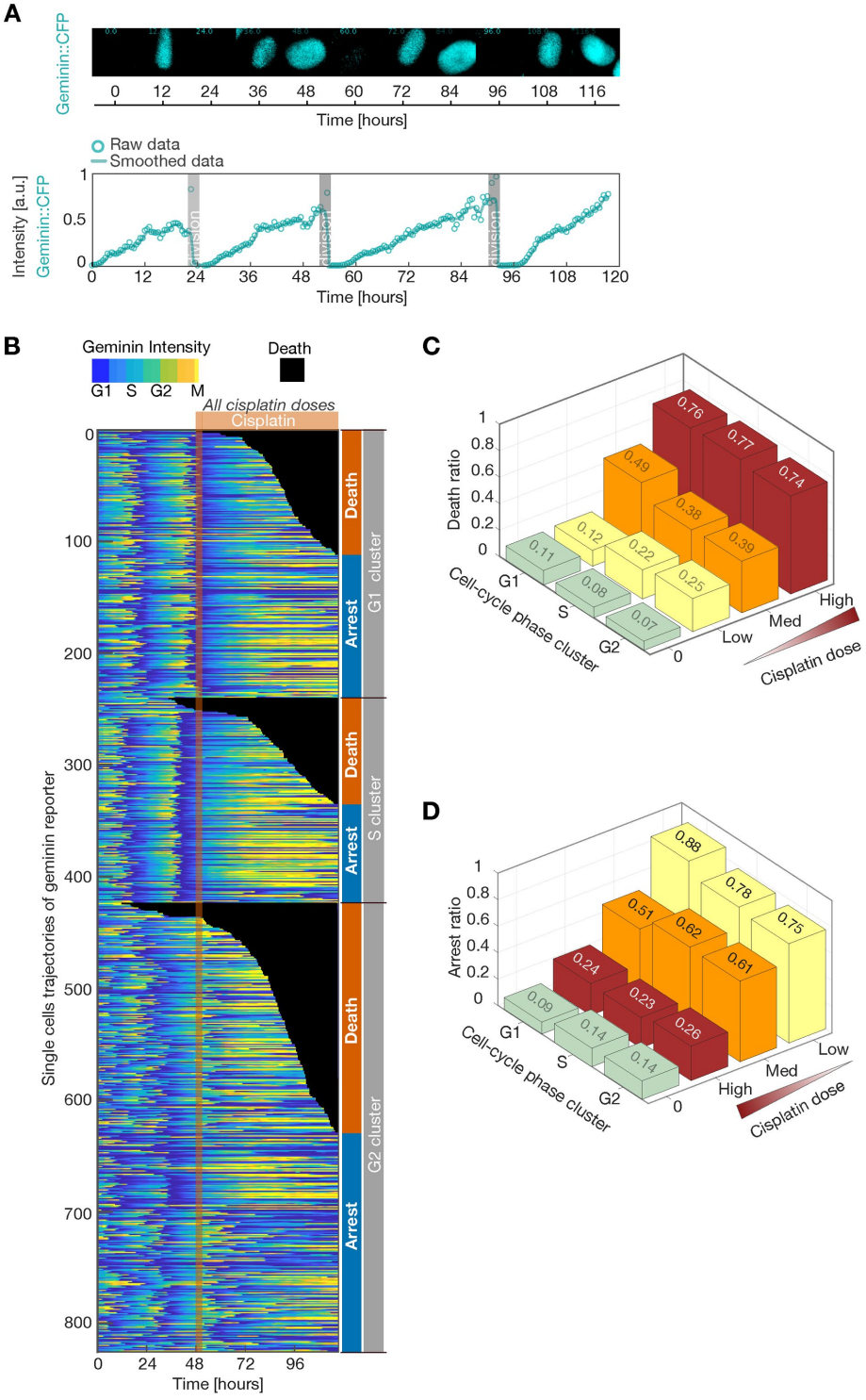

FIGURE 3: Cell cycle phase does not affect response to cisplatin. (A) Micrographs over time of a single cell carrying a Geminin-CFP fluorescent reporter (first row) with the corresponding Geminin trajectory (second row). Raw normalized data (circles) and smoothed normalized data (line) are shown. Division events are marked with a gray vertical bar. (B) Single-cell trajectories from cells treated with low, medium, and high doses were pooled ($n = 825$ cells) and clustered initially according to the cell cycle phase at the time of cisplatin treatment (red vertical line) and further clustered according to the cellular outcomes. Death subgroups were sorted by their time of death. (C, D) Bar plots of (C) death and (D) arrest ratios as a function of the cisplatin dose and cell cycle phase. Ratio values and sample size numbers for each cell cycle cluster and treatment condition are in Supplemental Table 1.

show that highly proliferative cells die later and are more resistant to cell death induced by low and medium cisplatin doses (Figure 4F), but they lose this resistance at higher cisplatin doses.

Two distinct mechanisms can explain the differential resistance observed in high- and low-proliferative cells. First, highly proliferating cells may acquire less damage from cisplatin treatment. Alternatively, they may receive the same amount of damage as low-proliferative cells but resolve it more efficiently. To distinguish between these two scenarios, we compared the extent of damage induced by cisplatin between low- and high-proliferative cells by quantifying the levels of cisplatin-induced DNA adducts in each group (Supplemental Figure S4, A–C). This analysis revealed that the two groups acquired similar amounts of cisplatin-induced damage (Supplemental Figure S4, A–C), arguing that the relatively high resistance of high-proliferative cells is not due to lower levels of DNA damage following cisplatin treatment. We next tested whether basal cellular damage (pre–cisplatin treatment) can be linked to proliferative index. We determined the levels of DNA damage by quantifying the number of γH2AX foci, a marker for DNA double–strand breaks, in untreated cells. We found that higher-proliferation cells exhibit on average a smaller number of DNA double-strand breaks (Supplemental Figure S4, D and E). This suggests that heterogeneous levels of basal DNA damage impact cells' proliferative states and their likelihood of dying in response to a DNA damage–inducing drug. Specifically, cells carrying larger numbers of basal DNA breaks proliferate less and are more susceptible to dying in response to the additional damage induced by cisplatin.

Cisplatin dose and proliferation state together regulate cellular outcomes

Our results suggested that cisplatin dose and proliferation state, but not cell cycle phase at the time of treatment, affect cellular outcomes. To rigorously quantify the extent to which these parameters individually and in combination affect cellular outcomes, we used information theory, which has been applied in a variety of areas of molecular systems biology. Mutual information (Box 1) has been used in the field of molecular systems biology to analyze the extent of cooperativity between genetic interactions in contributing to a phenotype (Anastassiou, 2007; Chanda *et al.*, 2007).

Signal transduction pathways in mammalian cells resemble prototypic information transmission systems that can be described in the framework of information theory (Gatenby and Frieden, 2007). Mutual information has been used to study how information from different concentrations of ligands is transmitted into the activity of transcription factors in the MAPK (Voliotis *et al.*, 2014), Ca^{2+} and NFKB (Selimkhanov *et al.*, 2014), and TGFβ/SMAD and p53 (Benary *et al.*, 2018) pathways. This information is limited to values below one bit (from 0 to 0.4 bits) when the static response is considered and is significantly higher (4–5 bits) when the dynamic response is considered. Of particular relevance to our approach, mutual information has been used to study how the initial state of the cell (i.e., the initial level of signaling proteins in the apoptosis pathway) plays a role in the death–survival outcome (Palaniappan *et al.*, 2017).

We classified three predictor variables—cisplatin dose, proliferation state, and cell cycle phase—and determined their individual contributions tow cellular outcomes (death or arrest; Figure 4G). In the context of mutual information on signaling pathways, Palaniappan *et al.* (2017) set a cutoff of 0.005 to consider a gene important for transmitting information on the outcome, a practice that we adopt here. The dose of cisplatin conveyed the highest mutual information (*I*(cisplatin,outcome) = 0.1514), with the proliferative state holding less information about the cellular outcomes (*I*(prolif.,outcome) = 0.0295). Little to no information was conveyed by the cell cycle phase (I(cell cycle, outcome) = 0.0008). Notably, even though the cell cycle phase and proliferation state are likely not independent of each other (for example, the fraction of G2 cells in the low-proliferation group is approximately twice that in the high-proliferation group; Supplemental Figure S3D), our analysis showed that they provided different amounts of information on cellular outcomes.

We next used partial information decomposition (PID) to identify unique information, redundancy, and synergy between pairs of predictor variables in determining cellular outcome (Box 1 and Table 2). PID has been used in neuroscience to model a neuron as a neural processor with two inputs (Wibral *et al.*, 2017), to investigate how multiple neuronal sources contribute to the correct prediction of a target variable during training of a neural network (Tax *et al.*, 2017), or to examine the spiking activity of distinct electrodes in a neural culture (Timme *et al.*, 2014). Applying this model to pairs of input variables, we found that measuring cell cycle phase together with either of the other two predictor variables (cisplatin dose or SSPI) did not provide any unique information on cellular outcome (Figure 4G and Table 2). In these two cases, the total information provided by the combination of cell cycle phase and dose, or cell cycle phase and SSPI, reduced to the unique information provided by either

BOX 1: Mutual information.

The foundational measure of mutual information is entropy (Cover and Thomas, 2005). The entropy of a discrete random variable X measures its uncertainty, that is, how unpredictable its value is, and is defined as:

$$H(X) = -\sum_{i=1}^{n} p(x_i)\log_2 p(x_i)$$

where X can take on the values $x_1, x_2, \ldots, x_n$, with the respective probabilities $p(x_1), p(x_2), \ldots, p(x_n)$. Entropy is measured in bits, is maximized when all outcomes are equally likely to occur (the uncertainty is at its greatest), and is equal to zero when the random variable can only take one predetermined value (the outcome is entirely predictable). Variables that have a greater number of possible outcomes show higher entropy; for example, the entropy of an evenly weighted coin, with two possible outcomes, heads and tails (1 bit) is lower than that of a fair die with six possible outcomes (2.59 bits). Mutual information (I) quantifies the amount of information provided about one variable (X) by knowing the value of the other (Y). Its physical meaning is "the reduction of the uncertainty of Y due to the knowledge of X" and is given by:

$$I(X;Y) = H(X) - H(X|Y)$$

where $H(X|Y)$ is the uncertainty of X given Y (see Supplemental Table 9 for definitions of equations used here). Mutual information is always a nonnegative quantity, where high mutual information indicates a large reduction in uncertainty; low mutual information indicates a small reduction; and zero mutual information between two random variables means the variables are independent of each other.

When two variables (X_1 and X_2) both convey mutual information about a third (S), one can wonder whether the prediction of S can be improved by simultaneous observation of X_1 and X_2. Partial information decomposition (PID; Williams and Beer, 2010) determines the mechanisms by which two variables interact to provide information on a set of outcomes. First, two variables, X_1 and X_2, could each provide unique information about the outcome. Second, they could provide redundant information, as seen in a situation where X_1 and X_2 are completely or partially overlapping. Redundancy is the information common to all sources, that is, the minimum information that any predictor provides, while taking into account that predictors may provide information about different outcomes of S. It accounts only for the quantity of information provided, and not for the nature of the information. Finally, X_1 and X_2 may provide synergistic information that is obtained only from the combination of both variables together. This dissection of $I(\{X_1, X_2\}, S)$ into intuitive components provides an insight into how dependencies are distributed among the variables. $I(\{X_1, X_2\},S)$ is written as:

$$I(\{X_1;X_2\};S) = \text{Unique}(X_1;S) + \text{Unique}(X_2;S) + \text{Synergy}(\{X_1;X_2\};S) + \text{Redundancy}(\{X_1;X_2\};S)$$

$$I(X_1;S) = \text{Unique}(X_1;S) + \text{Redundancy}(\{X_1;X_2\};S)$$

$$I(X_2;S) = \text{Unique}(X_2;S) + \text{Redundancy}(\{X_1;X_2\};S)$$

where each term represents what portion of information is provided 1) redundantly by X_1 and X_2 (information overlap), 2) uniquely by X_1 or X_2 alone (what information X_1 provides about S X_2 does not, and vice versa), or 3) synergistically by X_1 and X_2 together (X_1 and X_2 provide bonus information about S when both are known simultaneously).

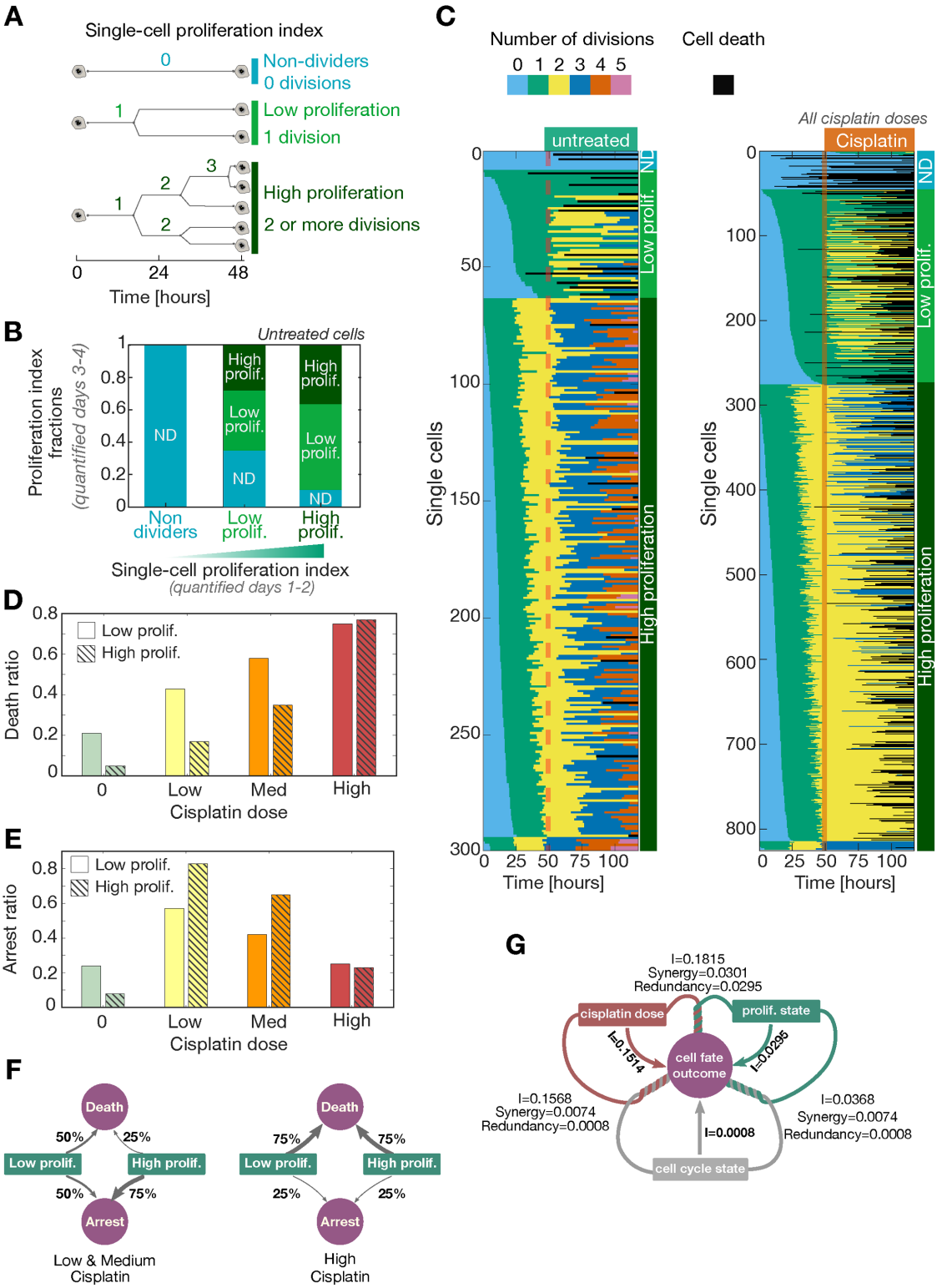

FIGURE 4: Single-cell proliferation index pretreatment modulates the response to cisplatin. (A) The number of divisions within the first 48 h defines three single-cell proliferation index categories: nondividers (0 divisions), low proliferation (1 division), and high proliferation (2 or more divisions). (B) Cells in each proliferation index category, as defined in the first 2 d of imaging, were monitored for an additional 2 d, and their proliferation index during this time period is shown. (C) Individual division profiles obtained after tracking cells for 5 d and annotating their division events. Left panel represents untreated cells, and right panel represents trajectories pooled from cells treated with low, medium, or high cisplatin doses, as defined in Figure 3. Each row represents the division activity of a single cell, with each mitotic or death event marked by a color transition (color code top left). Cells in each panel are clustered by their proliferation index before treatment and then sorted by their time of first mitosis. Cisplatin treatment was initiated after 2 d of unperturbed growth. Right side of each panel displays the corresponding single-cell proliferation index

Pred. X_1	Pred. X_2	Target S	Unique (X_1; S)	Unique (X_2; S)	Redund. ({X_1; X_2}; S)	Synergy ({X_1; X_2}; S)	I({X_1; X_2}; S)
Cycle	Dose	Cell out.	0.0	0.1506	0.0008	0.0054	0.1568
Cycle	Prol.	Cell out.	0.0	0.0287	0.0008	0.0075	0.0368
Prol.	Dose	Cell out.	0.0	0.1219	0.0295	0.0301	0.1815

The mutual information about a target variable S that is carried together by two predictor variables X_1 and X_2, I({X_1;X_2};S), is the sum of its four intuitive components: unique information carried by each variable separately, redundant information, and synergistic information.

TABLE 2: Partial information decomposition: basic quantities of information for different combinations of predictors X_1 and X_2 (cell cycle state, proliferative index, and cisplatin dose) and target variable cellular outcome S.

dose or SSPI alone. Interestingly, when cisplatin dose and proliferative index were measured together, only cisplatin dose provided unique information on cellular outcome. However, for this combination of predictor variables, the synergy and redundancy terms represent a significant portion of the total information conveyed (Figure 4G and Table 2). First, proliferative index and cisplatin dose may provide some overlapping information (Redundancy [prolif., dose] = 0.0295). Furthermore, some information is provided synergistically by the dose and proliferation index (Synergy [prolif., dose] = 0.0301), indicating that they are engaged in a complex interaction with cellular outcome. That is, the combination of dose and proliferative status might provide information on cellular outcome that is not available from either alone (synergy). Thus, to better predict the cellular outcome after cisplatin treatment, there is added information in simultaneously knowing the proliferative state and the cisplatin dose. This result is in accordance to our results in Figure 4F, where we observe that proliferative state and cisplatin dose together confer information on cellular outcome.

Information content on its own does not provide insights into how individual input variables influence the different cellular outcomes. By combining the results of the information content analysis with the ratios of distributions in Figures 3, C and D, and 4, D and E, we found that increasing cisplatin dose induced a switch from cell cycle arrest to cell death in both low– and high–proliferation index cells (Figure 4, D–G). Most interestingly, at low and medium cisplatin doses, the proliferative state of a cell influences the balance of cellular outcomes between cell cycle arrest and cell death (Figure 4F).

DISCUSSION

DNA damaging agents such as cisplatin are commonly used chemotherapeutics that show great variability in responses across and within tumors, often with a significant fraction of cells surviving treatment. Recent single-cell studies have revealed how nongenetic cell-to-cell variability can drive significant phenotypic differences in response to identical drug treatment (Snijder and Pelkmans, 2011; Paek *et al.*, 2016; Uphoff, 2018), leading to the hypothesis that the variability of cellular states might underlie the heterogeneous drug responses within a tumor. Here, we present a single-cell based analysis of two cellular features, the proliferation status and cell cycle phase, and determine their relationship with the individual cellular outcomes upon chemotherapy.

We first quantified the dynamics of population responses to a wide range of cisplatin concentrations. The strength of the DNA damage, together with the cellular state, is expected to modulate the survival and death response globally. Our time-resolved measurements revealed dose-dependent variations in the kinetics of population growth (Figure 1C), the underlying differences in the kinetics of death and cell division (Figure 1, D and E), and the effects of cisplatin dose on modulating the balance between cell death and cell cycle arrest (Figure 1G). Overall, we found that the cell cycle phase at the time of cisplatin treatment and/or the execution of cell division after treatment had minimal effects on the final cellular outcomes. The proliferation history leading up to the time of treatment, however, influenced cellular outcomes and showed partial synergy with the cisplatin dose in modulating the final outcomes. Specifically, we found that low-SSPI cells were more likely than high-SSPI cells to die at low to medium cisplatin doses, a result that was surprising in light of established correlations between low proliferation and resistance to chemotherapeutics (Remvikos *et al.*, 1989; Amadori *et al.*, 1997). Various cancer cell lines are known to exhibit great phenotypic variability in their response to DNA-damaging agents. Future studies comparing the relative contributions of proliferation status and cell-cycle phase to drug sensitivity across additional cell lines will reveal whether the significance of proliferation status observed in this study serves as a general paradigm for influencing drug sensitivity, or whether in other cell lines different aspects of internal cellular states govern the responses to DNA damage.

We found that cell cycle phase did modulate the probability of a cell dividing after cisplatin, as the G2 population showed the largest fraction of cells undergoing mitosis after cisplatin treatment. It is likely that the G2 cells that divide soon after treatment are past the G2 checkpoint and therefore are initially insensitive to cisplatin and proceed to mitosis. Among the population that divided, we also detected cells that divided very late, an unusual event for cells in other cell cycle phases. We have observed similar phenomena following DNA damage by gamma irradiation (Reyes *et al.*, 2018). Our results now suggest that G2 cells may be particularly prone to this outcome, which can generate catastrophic mitoses with genome fragmentation and micronucleus formation.

Intriguingly, we identified proliferation status as a cellular feature that operates independent of cell cycle phase to regulate responses to cisplatin. We found that low-proliferation cells were most susceptible to cell death, while high-proliferation cells were most likely to arrest. This finding was initially surprising to us, as the dominant description in the literature is that highly proliferative tumors are

category. ND: nondivider. (D, E) Death and arrest ratio bar plots grouped by cisplatin dose for cells with low and high proliferation index. Sample numbers per proliferation index and treatment condition are in Supplemental Table 1. (F) Cellular outcome percentages as a function of proliferative state and cisplatin dose. Thickness of arrows represents the ratio of a particular outcome. (G) Information theory calculations indicate synergy between proliferative state and cisplatin dose in predicting cellular outcome. Schematics displaying mutual information "I" between predictor variables (cisplatin dose, proliferation state, and cell cycle phase) and cell fate outcome. Synergistic and redundant contributions between pairs of predictors are also displayed.

more sensitive to chemotherapeutics (Lin, 1973; Valeriote and Putten, 1975; Stover *et al.*, 2016). However, we note some key differences between studies. Many of the previous studies compared proliferation status and drug resistance between fundamentally different cell types. For example, the drug resistance of a cell line specifically selected for this property may be linked to other changes (Nakamura *et al.*, 2015), such as expression of drug importers or exporters (Siddik, 2003), and only indirectly to proliferation rate per se. Similarly, cancer stem cells, which are typically slow-growing and drug-resistant, often express unique markers (compared with the total tumor population) and may even harbor unique genetic signatures, and thus their proliferation state and drug resistance may also be only indirectly correlated. Here we have studied *naturally occurring heterogeneity* in a clonal population and found that differences in proliferation rate can influence cellular outcomes. Note that U2OS cells are known to exhibit genomic instability, and their populations can be highly genetically heterogeneous. It is therefore possible that differences in cisplatin sensitivity result from genetic differences, as observed in primary cancer cells (Niehr *et al.*, 2018). However, since the cells in this work were recently derived from a single-cell clone, the probability of heterogeneity resulting from new genetic modifications is small. Furthermore, our observation that proliferation state is dynamic argues against the possibility of distinct genetic subpopulations influencing the response to cisplatin.

In addition to its role in cell death sensitivity, our data show that proliferation index also affects time of death (Supplemental Figure S3C). Variability in time of death has previously been reported in a clonal population of human cancer cells treated with the apoptosis-inducing ligand TRAIL (Spencer *et al.*, 2009). In this case, the variation arose from nongenetic heterogeneity in expression of factors in the receptor-mediated apoptosis pathway (BCL2 protein family). Here, we have observed variation in the extent of basal DNA damage between low- and high-proliferation cells (Supplemental Figure S4). It is possible that basal damage status impacts the expression of proapoptotic genes, thus affecting the probability and timing of death in response to cisplatin treatment. Further studies will be required to understand the molecular mechanism underlying the link between basal DNA damage, proliferative state, and cellular outcomes.

Understanding the final cellular outcomes is critical for determining appropriate chemotherapeutic regimens. We classified cells as "proliferative," "arrested," or "dead," based on tracking them for 3 d post–treatment with cisplatin. Thus, it is possible that cells classified as "arrested" might die or reenter the cell cycle at later times. However, population growth measurements under a wide range of doses and monitored 5 d posttreatment do not show signs of recovery past the third day posttreatment (Figure 1C). In addition, single-cell tracking shows that the fraction of dividing cells plateaus around 48 h posttreatment (Figure 1E), suggesting that cells are not exiting arrest subsequently. It is still possible that arrested cells might eventually die. Monitoring the timing and extent of death at late timepoints was not possible due to technology and experimental limitations of our setup, such as photodamage from imaging and overgrowth of cells.

Our results have potentially important implications for interpreting clinical measurements of proliferation. Our data suggest that in some circumstances slowly proliferating tumors might in fact be vulnerable to therapy. We find that cell cycle position per se does not appear to modify cellular outcomes upon treatment, which is consistent with the historical lack of success of strategies designed to modify proliferation and cell cycle status in cancer therapy with estrogenic recruitment—for example, Bontenbal *et al.* (2000); Paridaens *et al.* (1993). In the future, we anticipate that analyses similar to the one presented here, using more mechanistic live-cell markers, could provide potential targets that might be used to alter the proliferative state of cancer cells and "prime" them to therapy.

MATERIALS AND METHODS

Cell culture

U2OS cells (from ATCC HTB-96) were cultured in RPMI with L-glutamine (R8758 SIGMA) supplemented with 10% fetal bovine serum (FBS, Capricorn Scientific 12A) and 1% of antibiotic–antimycotic solution (GIBCO 15240096). All cultures were routinely tested for mycoplasma. Stable expression of a nuclear marker (mKate2-NLS) or a cell cycle reporter (CFP-hGeminin) was obtained by lentiviral transduction and subsequent clonal selection. In all experiments, we used freshly thawed and early passage clonal cells (P2-4). Cells were treated with Cisplatin (Sigma PHR1624) dissolved in NaCl solution at the indicated concentrations (0.1–70 μM). For imaging we used either 12-well plastic plates (Corning) or 24-well polymer coverslip coated plates (μ–Plate Ibidi coating treatment). For the microscopy experiments we used optimized live-cell fluorescence microscopy media (FluoroBrite ThermoFisher Scientific) supplemented with 10% FBS, 1% antibiotic–antimycotic solution, and L-glutamine 300 mg/l.

Microscopy

Time-lapse imaging was accomplished by a long-term low-resolution incubator-embedded microscope (Incucyte Essen Bioscience) and a high-resolution multichannel fluorescence microscope with an environmental chamber for cell culture (Widefield Ti2, Nikon), a 20× Plan Apo magnification. Analysis of images employed custom MATLAB code (Mathworks) and built-in Incucyte software. Results in Figure 1, B and Cm, and Supplemental Figure S1 were carried on the long-term low-resolution Incucyte incubator-embedded microscope. In these experiments, cells were seeded at 5% density 24 h before the beginning of the image acquisition. RPMI-based media was exchanged for FluoroBrite-based medium 1 h before the image acquisition started. Cisplatin was added to the media 48 h after the beginning of the image acquisition at the described doses in a 100-μl cisplatin-media solution (5% of total volume), and control cells remained untreated throughout the experiment. Two biological replicates per dose from independent plates and randomized well positions were used in these experiments. Cells carry the mKate2-NLS nuclear fluorescent marker to facilitate nuclei segmentation analysis and counting. Images were captured every 30 min. Frame-by-frame nucleus counting was carried out using the Incucyte image analysis software and further processed in MATLAB. See the example of representative Incucyte movies in the Supplements showing a composite of the bright field (gray-scale) and mKate2-NLS nuclear signal (red).

Results presented in Figures 1, D–G, and 2–4 and Supplemental Figures S2 and S3 were derived from experiments done in a high-resolution multichannel wide-field EPI fluorescence Nikon Ti2 microscope equipped with a live-cell incubator (Okolab), LED illumination (Lumencore, SpectraX), and sCMOS, PCO camera. Seeding, media changes, acquisition frame rate, and cisplatin treatment followed the same protocol described above, except that treatment began 49.5 h after the acquisition started. Control cells remained untreated and treated cells received cisplatin doses of 7, 10, and 13 μM, referred as low, medium, and high, respectively. The results for each condition originate from three technical replicates in different wells with an average of 12 randomized intrawell image positions per well. Cells were tracked from the beginning of the experiment ($t = 0$)

until the last time frame or the time of death. Upon cell division, only one of the daughter cells was followed. Cells that left the field of view were discarded from the analysis. We tracked a total of 300, 247, 262, and 316 individual cells for the control, low, medium, and high cisplatin doses, respectively. See representative NikonTi2 movies in the Supplements, showing a composite of the bright field (gray scale) and the CFP-hGeminin marker (cyan). Results presented in Supplemental Figures S4 and S5 were recorded using the same seeding conditions and Nikon Ti2 microscope as described above. A high dose of cisplatin (13 μM) was added to the cells at 48 h and cells were tracked for 6 h more and immediately fixed for immunostaining. We tracked 333 and 323 individual cells for the control and high cisplatin dose, respectively.

Immunofluorescence

Cells were fixed for 15 min at room temperature (RT) with 4% paraformaldehyde at the end of the live imaging recording. Cells were washed three times with 1X-PBS and then permeabilized with 0.1% Triton-X and blocked with 2% BSA in 1X-PBS. Cells were incubated 1 h at RT with primary antibody (1:500 dilution), washed three times with 1X-PBS, and stained with secondary fluorescent antibodies overnight at 4°C (1:2000 dilution). The next day, cells were washed three times with 1X-PBS and stained with 4′,6-diamidino-2-phenylindole (1:2000 dilution) for 2 h at RT, followed by a final wash with 1X-PBS. The primary antibodies used were an antiphosphohistone H2A.X (Ser139), clone JBW301 from Sigma-Aldrich and an anti-cisplatin DNA adducts antibody, clone ICR4 from Merck Millipore. The secondary antibodies used were Alexa Fluor 647 goat anti-rat and 488 donkey anti-mouse from Invitrogen. Cells were imaged the next day using the Nikon Ti2 microscope described previously.

Tracking and cell fate determination

Images were captured using the NIS-Elements AR software and exported as .tiff image files for tracking and analysis. Cells were tracked using semiautomated custom software developed specifically for cell fate annotation tracking of individual cells over long time scales as described in Reyes *et al.* (2018). This software provides individual cell tracking information, timing of division events, and timing of death identified visually as in Paek *et al.* (2016). Geminin-CFP reporter intensity was quantified using the tracking information from background subtracted images by averaging 10 pixels around the cell nucleus. Cells that died before the time of treatment initiation or escaped the field of view were discarded from the calculations of cell fate ratio posttreatment. Results presented in Supplemental Figures S4D andS5C integrate live and IF single-cell data. Intensities of nuclear values from the IF images were obtained using the same code from Reyes *et al.* (2018) from background-subtracted images averaging 20 pixels around the cell nucleus. Violin plots were made using the Matlab function distributionPlot.m as described in Jonas (2020).

Survival Kaplan–Meier estimates

In Figure 1, D and E, the fractions of dying and dividing cells were computed using the empirical cumulative distribution function implemented in the MATLAB "ecdf.m." Confidence intervals were estimated using Greenwood's formula. Dying fraction uses timing of death as the cumulative event. Right censoring was applied to cells where death events were not registered within the whole experiment. All tracked cells are considered in this analysis. Dividing fraction uses timing of first division after treatment as the cumulative event. Right censoring was applied to cells that did not experience a mitotic event nor die within the whole experiment. Only surviving cells are considered in this analysis; for example, cells that experienced a mitotic event but later died are not considered within our pool. The analysis extends until the last registered event in each condition, therefore the plots reach a plateau at different dose-dependent times.

Final cell fate fractions

Cells' fates are classified as described in Figure 1F within 3 d after treatment initiation. For each group, fractions are calculated as the ratio between the number of cells in each cell fate class to the total number of cells per treatment condition at the time of treatment initiation, so that for each treatment condition all cell fate fractions sum up to one (Figure 1G).

Intermitotic time distribution analysis

IMT is calculated as the time difference between consecutive manually annotated division events. For the analysis and fit of the histograms in Figure 2, we used the toolbox from MATLAB *Distrib.m* to fit distributions to a exponentially modified Gaussian (EMG) model (Lacouture and Cousineau, 2008).

Processing and clustering of CFP-Geminin traces

A one-dimensional median filter was applied to the raw geminin traces using the MATLAB function "medfilt1.m" with a time window of 3 h (smoothed traces). In Figure 3A, second-row traces are normalized using the maximum raw value within the whole experiment time (smoothed normalized traces). In Figure 3B, smoothed traces from the low, medium, and high cisplatin doses are clustered in three groups based on the cross-correlation between traces in a time window of 16 h before treatment initiation. Linkage clustering with a "ward" minimum variance algorithm and cross-correlation distance function was implemented in MATLAB using the functions "linkage.m," "finddelay.m," and "cluster.m," respectively. Within each cluster traces, were further grouped by their annotated cell fates, with death cells sorted by their time of death. Death cells before treatment are included in Figure 3B but disregarded for the ratio calculations in Figure 3, C and D. All individual smoothed normalized traces from each cluster are plotted in Supplemental Figure S2A, first row, as thin gray lines and a single representative trace as a thick red line.

Histogram plots in Supplemental Figure S2A, second row, show the density histogram of division events with treated (orange) and untreated cells (gray) using the clustering from the Geminin traces from Figure 3B.

Cell fate ratios

Cell fate ratios are calculated for each treatment dose in combination with cell cycle phase cluster (Figure 3, C and D) or single-cell proliferation index (Figure 4, D and E) as described in the following equation, generating 12 ratios:

$$\text{Cell fate ratio}_{i,j} = \frac{\text{Nr. cells in specific cell fate after treatment}_{i,j}}{\text{Total number of cells before treatment}_{i,j}}$$

subindex i: Control, low medium, and high cisplatin doses.
subindex j: Cell cycle cluter (G1, S and G2) or proliferation index (low, med, and high).

Division profile maps: Cells are clustered by their total number of divisions and then sorted by the time of first division. Each division event is marked with a color change at the time of division, as shown in Figure 4C. Cell death is marked with black and treatment initiation is shown by a vertical orange line.

Error estimation: In the supplemental tables, ratio errors are estimated using the binomial 95% confidence intervals calculation as follows:

$$\text{Estimated error} = z\sqrt{\frac{\hat{p}(1-\hat{p})}{n}}$$

$\hat{p}$: cell fate likehood
n: number of samples in subcluster
z: 1-0.95 for the 95% confidence interval

In the supplemental tables we provide all ratio values and errors and a set of tables with the absolute numbers per condition, thus providing all the data to explore alternative error calculations and statistical tests.

Code availability

The p53Cinema software package for tracking and quantifying single-cell data can be downloaded at https://github.com/balvahal/p53CinemaManual. All additional custom MATLAB code can be provided upon request.

ACKNOWLEDGMENTS

We thank Manuela Benary, Torsten Gross, and Stefan Florian for stimulating discussions and constructive criticism. We thank members of the Reber, Blüthgen, and Lahav labs for comments and helpful advice. We thank Stefanie Scharf and Nicole Steindorf-Rentzsch for administrative support. We thank the AMBIO imaging facility (Charité, Berlin) for support with live-cell imaging. This research was supported by the IRI Life Sciences independent postdoctoral fellowship from the Humboldt-Universität zu Berlin (Excellence Initiative—Deutsche Forschungsgemeinschaft) and National Institutes of Health Grants GM116864 and GM083303 (to G.L.) and 4R00CA297727-03 (to J.S.-O). A.E.G. was also supported by Susan G. Komen for the Cure (PDF15331988) and the Joachim Herz Stiftung.

REFERENCES

Albeck JG, Burke JM, Aldridge BB, Zhang M, Lauffenburger DA, Sorger PK (2008). Quantitative analysis of pathways controlling extrinsic apoptosis in single cells. Mol Cell 30, 11–25.

Amadori D, Volpi A, Maltoni R, Nanni O, Amaducci L, Amadori A, Giunchi DC, Vio A, Saragoni A, Silvestrini R (1997). Cell proliferation as a predictor of response to chemotherapy in metastatic breast cancer: a prospective study. Breast Cancer Res Treat 43, 7–14.

Anastassiou D (2007). Computational analysis of the synergy among multiple interacting genes. Mol Syst Biol 3, 83.

Arora M, Moser J, Phadke H, Basha AA, Spencer SL (2017). Endogenous replication stress in mother cells leads to quiescence of daughter cells. Cell Rep 19, 1351–1364.

Baguley BC, Marshall ES, Whittaker JR, Dotchin MC, Nixon J, McCrystal MR, Finlay GJ, Matthews JHL, Holdaway KM, van Zijl P (1995). Resistance mechanisms determining the in vitro sensitivity to paclitaxel of tumour cells cultured from patients with ovarian cancer. Eur J Cancer 31, 230–237.

Benary M, Nolis I, Blüthgen N, Loewer A (2018). Information flow in a mammalian signal transduction pathway. In: Information and Communication Theory in Molecular Biology, ed. M Bossert, Lecture Notes in Bioengineering, Cham, Switzerland: Springer, 101–114.

Berenbaum MC (1972). In vivo determination of the fractional kill of human tumor cells by chemotherapeutic agents. Cancer Chemother Rep 56, 563–571.

Bontenbal M, van Putten WLJ, Burghouts JTM, Baggen MGA, Ras GJ, Stiegelis WF, Beudeker M, Janssen JTP, Braun JJ, van der Linden GHM, *et al.* (2000). Value of estrogenic recruitment before chemotherapy: first randomized trial in primary breast cancer. J Clin Oncol 18, 734–742.

Chakrabarti S, Paek AL, Reyes J, Lasick KA, Lahav G, Michor F (2018). Hidden heterogeneity and circadian-controlled cell fate inferred from single cell lineages. Nat Commun 9, 1–13.

Chanda P, Zhang A, Brazeau D, Sucheston L, Freudenheim JL, Ambrosone C, Ramanathan M (2007). Information-theoretic metrics for visualizing gene–environment interactions. Am J Hum Genet 81, 939–963.

Chatzopoulou EI, Raharja-Liu P, Murschhauser A, Sekhavati F, Buggenthin F, Vollmar AM, Marr C, Rädler JO (2018). A single-cell micro-trench platform for automatic monitoring of cell division and apoptosis after chemotherapeutic drug administration. Nat Sci Rep 8, 1–10.

Cover TM, Thomas JA (2005). Elements of Information Theory, Hoboken, NJ: Wiley.

Driessens G, Beck B, Caauwe A, Simons BD, Blanpain C (2012). Defining the mode of tumour growth by clonal analysis. Nature 488, 527–530.

Fumagalli M, Rossiello F, Clerici M, Barozzi S, Cittaro D, Kaplunov JM, Bucci G, Dobreva M, Matti V, Beausejour CM, *et al.* (2012). Telomeric DNA damage is irreparable and causes persistent DNA-damage-response activation. Nat Cell Biol 14, 355–365.

Galluzzi L, Senovilla L, Vitale I, Michels J, Martins I, Kepp O, Castedo M, Kroemer G (2012). Molecular mechanisms of cisplatin resistance. Oncogene 31, 1869–1883.

Gatenby RA, Frieden BR (2007). Information theory in living systems, methods, applications, and challenges. Bull Math Biol 69, 635–657.

Hafner M, Niepel M, Chung M, Sorger PK (2016). Growth rate inhibition metrics correct for confounders in measuring sensitivity to cancer drugs. Nat Methods 13, 521–527.

Hanahan D, Weinberg RA (2011). Hallmarks of cancer: the next generation. Cell 144, 646–674.

He G, Kuang J, Khokhar AR, Siddik ZH (2011). The impact of S- and G2-checkpoint response on the fidelity of G1-arrest by cisplatin and its comparison to a non-cross-resistant platinum(IV) analog. Gynecol Oncol 122, 402–409.

Hill BT, Baserga R (1975). The cell cycle and its significance for cancer treatment. Cancer Treat Rev 2, 159–175.

Hoshino T, Wilson CB, Rosenblum ML, Barker M (1975). Growth fraction and cell cycle time. 43, 127–135.

Inde Z, Dixon SJ (2018). The impact of non-genetic heterogeneity on cancer cell death. Crit Rev Biochem Mol Biol 53, 99–114.

Jonas (2020). Violin plots for plotting multiple distributions (distributionPlot.m). Matlabcentral. Available at: https://www.mathworks.com/matlabcentral/fileexchange/23661-violin-plots-for-plotting-multiple-distributions-distributionplot-m.

Korsnes MS, Korsnes R (2018). Single-cell tracking of A549 lung cancer cells exposed to a marine toxin reveals correlations in pedigree tree profiles. Front Oncol 8, 260.

Lacouture Y, Cousineau D (2008). How to use MATLAB to fit the ex-Gaussian and other probability functions to a distribution of response times. Tutor Quant Methods Psychol 4, 35–45.

Lin HS (1973). Differential lethal effect of cytotoxic agents on proliferating and nonproliferating lymphoid cells. Cancer Res 33, 1716–1720.

Luce RD (1986). Response Times: Their Role in Inferring Elementary Mental Organization, Oxford, UK: Oxford University Press.

Luong KV, Wang L, Roberts BJ, Wahl JK, Peng A (2016). Cell fate determination in cisplatin resistance and chemosensitization. Oncotarget 7, 23383–23394.

Martins I, Raza SQ, Voisin L, Dakhli H, Allouch A, Law F, Sabino D, De Jong D, Thoreau M, Mintet M, *et al.* (2018). Anticancer chemotherapy and radiotherapy trigger both non-cell-autonomous and cell-autonomous death article. Cell Death Dis 9, 716.

Mitchison TJ (2012). The proliferation rate paradox in antimitotic chemotherapy. Mol Biol Cell 23, 1–6.

Nakamura T, Shinriki S, Jono H, Guo J, Ueda M, Hayashi M, Yamashita S, Zijlstra A, Nakayama H, Hiraki A, *et al.* (2015). Intrinsic TGF-β2-triggered SDF-1-CXCR4 signaling axis is crucial for drug resistance and a slow-cycling state in bone marrowdisseminated tumor cells. Oncotarget 6, 1008–1019.

Niehr F, Eder T, Pilz T, Konschak R, Treue D, Klauschen F, Bockmayr M, Türkmen S, Jöhrens K, Budach V, *et al.* (2018). Multilayered omics-based analysis of a head and neck cancer model of cisplatin resistance reveals intratumoral heterogeneity and treatment-induced clonal selection. Clin Cancer Res 24, 158–168.

Noguchi S (2006). Predictive factors for response to docetaxel in human breast cancers. Cancer Sci 97, 813–820.

Noll DM, McGregor Mason T, Miller PS (2006). Formation and repair of interstrand cross-links in DNA. Chem Rev 106, 277–301.

Paek AL, Liu JC, Forrester WC, Lahav G, Paek AL, Liu JC, Loewer A, Forrester WC, Lahav G (2016). Cell-to-cell variation in p53 dynamics leads to fractional killing. Cell 165, 631–642.

Palaniappan SK, Bertaux F, Pichen M, Fabre E, Batt G, Genest B (2017). Abstracting the dynamics of biological pathways using information theory: a case study of apoptosis pathway. Bioinformatics 33, 1980–1986.
Paridaens R, Heuson JC, Julien JP, Veyret C, Van Zyl J, Klijn JGM, Sylvester R, Mignolet F (1993). Assessment of estrogenic recruitment before chemotherapy in advanced breast cancer: a double-blind randomized study. European Organization for Research and Treatment of Cancer Breast Cancer Cooperative Group. J Clin Oncol 11, 1723–1728.
Remvikos Y, Beuzeboc P, Zajdela A, Voillemot N, Magdelenat H, Pouillart P (1989). Correlation of pretreatment proliferative activity of breast cancer with the response to cytotoxic chemotherapy. JNCI J Natl Cancer Inst 81, 1383–1387.
Reyes J, Chen JY, Stewart-Ornstein J, Karhohs KW, Mock CS, Lahav G (2018). Fluctuations in p53 signaling allow escape from cell-cycle arrest. Mol Cell 71, 581–591.e5.
Rupniak HT, Whelan RDH, Hill BT (1983). Concentration and time-dependent inter-relationships for antitumour drug cytotoxicities against tumour cells in vitro. Int J Cancer 32, 7–12.
Ryl T, Kuchen EE, Bell E, Shao C, Flórez AF, Mönke G, Gogolin S, Friedrich M, Lamprecht F, Westermann F, *et al*. (2017). Cell-cycle position of single MYC-driven cancer cells dictates their susceptibility to a chemotherapeutic drug. Cell Syst 5, 237–250.e8.
Sakaue-Sawano A, Kurokawa H, Morimura T, Hanyu A, Hama H, Osawa H, Kashiwagi S, Fukami K, Miyata T, Miyoshi H, *et al*. (2008). Visualizing spatiotemporal dynamics of multicellular cell-cycle progression. Cell 132, 487–498.
Selimkhanov J, Taylor B, Yao J, Pilko A, Albeck J, Hoffmann A, Tsimring L, Wollman R (2014). Accurate information transmission through dynamic biochemical signaling networks. Science 346, 1370–1373.
Sharma SV, Lee DY, Li B, Quinlan MP, Takahashi F, Maheswaran S, McDermott U, Azizian N, Zou L, Fischbach MA, *et al*. (2010). A chromatin-mediated reversible drug-tolerant state in cancer cell subpopulations. Cell 141, 69–80.
Shen H, Perez RE, Davaadelger B, Maki CG (2013). Two 4N cell-cycle arrests contribute to cisplatin-resistance. PLoS One 8, 2–9.
Siddik ZH (2003). Cisplatin: mode of cytotoxic action and molecular basis of resistance. Oncogene 22, 7265–7279.
Sigal A, Milo R, Cohen A, Geva-Zatorsky N, Klein Y, Liron Y, Rosenfeld N, Danon T, Perzov N, Alon U (2006). Variability and memory of protein levels in human cells. Nature 444, 643–646.
Snijder B, Pelkmans L (2011). Origins of regulated cell-to-cell variability. Nat Rev Mol Cell Biol 12, 119–125.
Spencer SL, Gaudet S, Albeck JG, Burke JM, Sorger PK (2009). Non-genetic origins of cell-to-cell variability in TRAIL-induced apoptosis. Nature 459, 428–432.
Stover DG, Coloff JL, Barry WT, Brugge JS, Winer EP, Selfors LM (2016). The role of proliferation in determining response to neoadjuvant chemotherapy in breast cancer: a gene expression-based meta-analysis. Clin Cancer Res 22, 6039–6050.
Tannock I (1978). Cell kinetics and chemotherapy: a critical review. Cancer Treat Rep 62, 1117–1133.
Tax TMS, Mediano PAM, Shanahan M (2017). The partial information decomposition of generative neural network models. Entropy 19, 474.
Timme N, Alford W, Flecker B, Beggs JM (2014). Synergy, redundancy, and multivariate information measures: an experimentalist's perspective. J Comput Neurosci 36, 119–140.
Tubiana M, Pejovic MH, Chavaudra N, Contesso G, Malaise EP (1984). The long-term prognostic significance of the thymidine labelling index in breast cancer. Int J Cancer 33, 441–445.
Tyson DR, Garbett SP, Frick PL, Quaranta V (2012). Fractional proliferation: a method to deconvolve cell population dynamics from single-cell data. Nat Methods 9, 923–928.
Uphoff S (2018). Real-time dynamics of mutagenesis reveal the chronology of DNA repair and damage tolerance responses in single cells. Proc Natl Acad Sci USA 115, E6516–E6525.
Valeriote F, Putten LV (1975). Proliferation-dependent cytotoxicity of anticancer agents: a review. Cancer Res 35, 2619–2630.
Voliotis M, Perrett RM, McWilliams C, McArdle CA, Bowsher CG (2014). Information transfer by leaky, heterogeneous, protein kinase signaling systems. Proc Natl Acad Sci USA 111, E326–E333.
Wibral M, Priesemann V, Kay JW, Lizier JT, Phillips WA (2017). Partial information decomposition as a unified approach to the specification of neural goal functions. Brain Cogn 112, 25–38.
Williams PL, Beer RD (2010). Nonnegative decomposition of multivariate information. ArXiv 10042515.
Wolff SC, Kedziora KM, Dumitru R, Dungee CD, Zikry TM, Beltran AS, Haggerty RA, Cheng J, Redick MA, Purvis JE (2018). Inheritance of OCT4 predetermines fate choice in human embryonic stem cells. Mol Syst Biol 14, e8140.
Yano S, Zhang Y, Miwa S, Tome Y, Hiroshima Y, Uehara F, Yamamoto M, Suetsugu A, Kishimoto H, Tazawa H, *et al*. (2014). Spatial-temporal FUCCI imaging of each cell in a tumor demonstrates locational dependence of cell cycle dynamics and chemoresponsiveness. Cell Cycle 13, 2110–2119.
Zamble DB, Lippard SJ (1995). Cisplatin and DNA repair in cancer chemotherapy. Trends Biochem Sci 20, 435–439.